

# WATER ICE LINES AND THE FORMATION OF GIANT MOONS AROUND SUPER-JOVIAN PLANETS

RENÉ HELLER<sup>1,2</sup> AND RALPH PUDRITZ<sup>1</sup>

Origins Institute, McMaster University, Hamilton, ON L8S 4M1, Canada  
rheller@physics.mcmaster.ca, pudritz@physics.mcmaster.ca

Draft version June 26, 2021

## ABSTRACT

Most of the exoplanets with known masses at Earth-like distances to Sun-like stars are heavier than Jupiter, which raises the question of whether such planets are accompanied by detectable, possibly habitable moons. Here we simulate the accretion disks around super-Jovian planets and find that giant moons with masses similar to Mars can form. Our results suggest that the Galilean moons formed during the final stages of accretion onto Jupiter, when the circumjovian disk was sufficiently cool. But in contrast to other studies, we show that Jupiter was still feeding from the circumsolar disk and that its principal moons cannot have formed after the complete photoevaporation of the circumsolar nebula. To counteract the steady loss of moons into the planet due to type I migration, we propose that the water ice line around Jupiter and super-Jovian exoplanets acted as a migration trap for moons. Heat transitions, however, cross the disk during the gap opening within  $\approx 10^4$  yr, which makes them inefficient as moon traps. This indicates a fundamental difference between planet and moon formation. We find that icy moons larger than the smallest known exoplanet can form at about 15 - 30 Jupiter radii around super-Jovian planets. Their size implies detectability by the *Kepler* and *PLATO* space telescopes as well as by the *European Extremely Large Telescope*.

*Keywords:* accretion disks – planets and satellites: formation – planets and satellites: gaseous planets – planets and satellites: physical evolution – planet-disk interactions

## 1. CONTEXT

While thousands of planets and planet candidates have been found outside the solar system, some of which are as small as the Earth's moon (Barclay et al. 2013), no moon around an exoplanet has yet been observed. But if they transit their host stars, large exomoons could be detectable in the data from the *Kepler* space telescope or from the upcoming *PLATO* mission (Kipping et al. 2012; Heller 2014). Alternatively, if a large moon transits a self-luminous giant planet, the moon's planetary transit might be detectable photometrically or even spectroscopically, for example with the *European Extremely Large Telescope* (Heller & Albrecht 2014). It is therefore timely to consider models for exomoon formation.

Large moons can form in the dusty gas disks around young, accreting gas giant planets. Current models of moon formation either posit that most proto-satellites are rapidly lost into the planet by type I migration (Pollack & Reynolds 1974; Canup & Ward 2002; Mosqueira & Estrada 2003; Canup & Ward 2006; Sasaki et al. 2010) or that they drift outwards as they are fed from the spreading circumplanetary ring (Crida & Charnoz 2012). While H<sub>2</sub>O ice lines act as planet traps that halt rapid type I migration in circumstellar disks (Kretke & Lin 2007; Hasegawa & Pudritz 2011, 2012), this trap mechanism has not been considered in theories of moon formation so far. The position of the water (H<sub>2</sub>O) condensation ice line has sometimes been modeled ad hoc (Sasaki et al. 2010) to fit the H<sub>2</sub>O distribution in the Galilean moon system (Mosqueira & Estrada 2003). We here model the temperature evolution in the accretion disks around Jo-

vian planets and find evidence that Jupiter's H<sub>2</sub>O ice line has worked as a moon trap for Ganymede.

There are several reasons why water ice lines could play a fundamental role in the formation of giant moons. The total mass of a giant planet's moon system is sensitive to the location of the H<sub>2</sub>O ice line in the circumplanetary disks, where the surface density of solids ( $\Sigma_s$ ) increases by about factor of three (Hayashi 1981), because the mass of the fastest growing object is proportional to  $\Sigma_s^{3/2}$ . This suggests that the most massive moons form at or beyond the ice line. In this regard, it is interesting that the two lightest Galilean satellites, Io (at 6.1 Jupiter radii [ $R_{\text{Jup}}$ ] from the planetary core) and Europa (at 9.7  $R_{\text{Jup}}$ ), are mostly rocky with bulk densities  $> 3 \text{ g cm}^{-3}$ , while the massive moons Ganymede (at 15.5  $R_{\text{Jup}}$ ) and Callisto (at 27.2  $R_{\text{Jup}}$ ) have densities below  $2 \text{ g cm}^{-3}$  and consist by about 50% of H<sub>2</sub>O (Showman & Malhotra 1999). It has long been hypothesized that Jupiter's circumplanetary disk dissipated when the ice line was between the orbits of Europa and Ganymede, at about 10 to 15  $R_{\text{Jup}}$  (Pollack & Reynolds 1974). Moreover, simulations of the orbital evolution of accreting proto-satellites in viscously dominated disks around Jupiter, Saturn, and Uranus indicate a universal scaling law for the total mass of satellite systems ( $M_{\text{T}}$ ) around the giant planets in the solar system (Canup & Ward 2006; Sasaki et al. 2010), where  $M_{\text{T}} \approx 10^{-4}$  times the planetary mass ( $M_{\text{p}}$ ).

## 2. METHODS

In the Canup & Ward (2002) and the Mosqueira & Estrada (2003) models, the accretion rate onto Jupiter was assumed to be time-independent. Canup & Ward (2006) focussed on the migration and growth of proto-moons, but they did not describe their assumptions for the temperature profile in the planetary accretion disk.

<sup>1</sup> Department of Physics and Astronomy, McMaster University

<sup>2</sup> Postdoctoral fellow of the Canadian Astrobiology Training Program

Others used analytical descriptions for the temporal evolution of the accretion rates or for the movement of the H<sub>2</sub>O ice lines (Makalkin & Dorofeeva 1995; Mousis & Gautier 2004; Canup & Ward 2006; Sasaki et al. 2010; Ogihara & Ida 2012) or they did not consider all the energy inputs described above (Alibert et al. 2005).

We here construct, for the first time, a semi-analytical model for the circumplanetary accretion disks of Jovian and super-Jovian planets that is linked to pre-computed planet evolution tracks and that contains four principal contributions to the disk heating: (i) viscous heating, (ii) accretion onto the circumplanetary disk, (iii) planetary irradiation, and (iv) heating from the ambient circumstellar nebula. Compared to previous studies, this setup allows us to investigate many scenarios with comparatively low computational demands, and we naturally track the radial movement of the H<sub>2</sub>O ice line over time. This approach is necessary, because we do not know any extrasolar moons that could be used to calibrate analytical descriptions for movement of the ice line around super-Jovian planets. We focus on the large population of Jovian and super-Jovian planets at around 1 AU from Sun-like stars, several dozens of which had their masses determined through the radial velocity technique as of today.

### 2.1. Disk Model

The disk is assumed to be axially symmetric and in hydrostatic equilibrium. We consider the dusty gas disks around young ( $\approx 10^6$  yr old), accreting giant planets with final masses beyond that of Jupiter ( $M_{\text{Jup}}$ ). These planets accrete gas and dust from the circumstellar disk. Their accretion becomes increasingly efficient, culminating in the so-called runaway accretion phase when their masses become similar to that of Saturn (Lissauer et al. 2009; Mordasini 2013). Once they reach about a Jovian mass (depending on their distance to the star, amongst others), they eventually open up a gap in the circumstellar disk and their accretion rates drop rapidly. Hence, the formation of moons, which grow from the accumulation of solids in the circumplanetary disks, effectively stops at this point or soon thereafter.

In our disk model, the radial extent of the inner, optically thick part of the circumplanetary disk, where moon formation is suspected to occur, is set by the disk's centrifugal radius ( $r_c$ ). At that distance to the planet, centrifugal forces on an object with specific angular momentum  $j$  are balanced by the planet's gravitational force. An analytical fit to 3D simulations of the disk around forming super-Jovian planets yields (Machida et al. 2008)

$$j(t) = \begin{cases} 7.8 \times 10^{11} \left( \frac{M_p(t)}{M_{\text{Jup}}} \right) \left( \frac{a_{*p}}{1 \text{ AU}} \right)^{7/4} \text{ m}^2 \text{ s}^{-1} & \text{for } M_p < M_{\text{Jup}} \\ 9.0 \times 10^{11} \left( \frac{M_p(t)}{M_{\text{Jup}}} \right)^{2/3} \left( \frac{a_{*p}}{1 \text{ AU}} \right)^{7/4} \text{ m}^2 \text{ s}^{-1} & \text{for } M_p \geq M_{\text{Jup}} \end{cases}, \quad (1)$$

where we introduced the variable  $t$  to indicate that the planetary mass ( $M_p$ ) evolves in time. The centrifugal

radius is then given by

$$r_{\text{cf}} = \frac{j^2}{GM_p}, \quad (2)$$

with  $G$  as Newton's gravitational constant. For Jupiter, this yields a centrifugal radius of  $21.68 R_{\text{Jup}}$ , which is slightly less than the orbital radius of the outermost Galilean satellite, Callisto, at  $27.22 R_{\text{Jup}}$ . This discrepancy is due to thermal effects that are neglected in the 3D disk model (Machida et al. 2008). We multiply the right-hand side of Equation (2) by a factor of  $27.22/21.68$  to include Callisto at the outer edge of the optically thick part of the disk and make our predictions consistent with the Jovian satellite system.

The disk is assumed to be mostly gaseous with a dust-to-mass fraction  $X$  (set to 0.006 in our simulations, Hasegawa & Pudritz 2013) and a constant Planck opacity  $\kappa_p$ . Although  $\kappa_p$  is fixed in any of our simulations, we tested various values. The fraction of the planetary light that contributes to the heating of the disk surface is parameterized by a coefficient  $k_s$ , typically between 0.1 and 0.5 (Makalkin & Dorofeeva 2014). This quantity must not be confused with the disk albedo, which can take values between almost 0 and 0.9, depending on the wavelength and the grain properties (D'Alessio et al. 2001). The sound velocity in the hydrogen (H) and helium (He) disk gas usually depends on the mean molecular weight ( $\mu$ ) and the temperature of the gas, but in the disk midplane it can be approximated (Keith & Wardle 2014) as  $c_s = 1.9 \text{ km s}^{-1} \sqrt{T_m(r)/1000 \text{ K}}$  for midplane temperatures  $T_m \lesssim 1000 \text{ K}$ . At these temperatures, ionization can be neglected and  $\mu = 2.34 \text{ kg mol}^{-1}$ . Further, the disk viscosity is given by  $\nu = \alpha c_s^2 / \Omega_K(r)$ , with  $\alpha$  as the viscosity parameter ( $10^{-3}$  in our simulations) and  $\Omega_K(r) = \sqrt{GM_p/r^3}$  as the Keplerian orbital frequency.

The steady-state gas surface density ( $\Sigma_g$ ) in the optically thick part of the disk can be obtained by solving the continuity equation for the infalling gas at the disk's centrifugal radius (Canup & Ward 2006), which yields

$$\Sigma_g(r) = \frac{\dot{M}}{3\pi\nu} \times \frac{\Lambda(r)}{l} \quad (3)$$

where

$$\Lambda(r) = 1 - \frac{4}{5} \sqrt{\frac{r_c}{r_d}} - \frac{1}{5} \left( \frac{r}{r_c} \right)^2$$

$$l = 1 - \sqrt{\frac{R_p}{r_d}} \quad (4)$$

is derived from a continuity equation for the infalling material and based on the angular momentum delivered to the disk (Canup & Ward 2006; Makalkin & Dorofeeva 2014), and  $\dot{M}$  is the mass accretion rate through the circumplanetary disk, assumed to be equal to the mass dictated by the pre-computed planet evolution models (Mordasini 2013). We parameterize  $r_d = R_H/5$ , where  $R_H$  is the planetary Hill radius, which yields  $r_d \approx 154 R_{\text{Jup}}$  for Jupiter (Sasaki et al. 2010; Makalkin & Dorofeeva 2014).

The effective half-thickness of the homogeneous flared disk, or its scale height, is derived from the solution of

the vertical hydrostatic balance equation as

$$h(r) = \frac{c_s(T_m(r))r^{3/2}}{\sqrt{GM_p}} . \quad (5)$$

We adopt the standard assumption of vertical hydrostatic balance in the disk and assume that the gas density ( $\rho_g$ ) in the disk decreases exponentially with distance from the midplane as per

$$\rho_g(r) = \rho_0 e^{\frac{-z^2}{2h(r)^2}} \quad (6)$$

where  $z$  is the vertical coordinate and  $\rho_0$  the gas density in the disk midplane. The gas surface density is given by vertical integration over  $\rho(r, z)$ , that is,

$$\Sigma_g(r) = \int_{-\text{inf}}^{+\text{inf}} dz \rho(r, z) . \quad (7)$$

Inserting Equation (6) into Equation (7), the latter can be solved for  $\rho_0$  and we obtain

$$\rho_0(r) = \sqrt{\frac{2}{\pi}} \frac{\Sigma_g(r)}{2h(r)} , \quad (8)$$

which only depends on the distance  $r$  to the planet. At the radiative surface level of the disk, or photospheric height ( $z_s$ ), the gas density equals

$$\rho_s(r) = \rho_0 e^{\frac{-z_s^2}{2h(r)^2}} \quad (9)$$

where we calculate  $z_s$  as

$$z_s(r) = \text{erf}^{-1}\left(1 - \frac{2}{3} \frac{\Sigma_g(r)}{\Sigma_g(r)\kappa_P}\right) \sqrt{2}h(r) . \quad (10)$$

The latter formula is derived using the definition of the disk's optical depth

$$\tau = \int_{z_s}^{+\text{inf}} dz \kappa_P \rho(r, z) = \kappa_P \int_{z_s}^{+\text{inf}} dz \rho(r, z) \quad (11)$$

and our knowledge of  $\tau = 2/3$  at the radiating surface level of the disk, which gives

$$\begin{aligned} \frac{2}{3} &= \kappa_P \int_{z_s}^{+\text{inf}} dz \rho_g(r, z) \\ \Leftrightarrow z_s(r) &= \text{erf}^{-1}\left(1 - \frac{2}{3} \sqrt{\frac{2}{\pi}} \frac{1}{h(r)\rho_0(r)\kappa_P}\right) \sqrt{2}h(r) . \end{aligned} \quad (12)$$

Using Equation (8) for  $\rho_0(r)$  in Equation (12), we obtain Equation (10).

Following the semi-analytical disk model of [Makalkin & Dorofeeva \(2014\)](#), the disk surface temperature is given by the energy inputs of various processes as per

$$\begin{aligned} T_s(r) &= \left( \frac{1 + (2\kappa_P \Sigma_g(r))^{-1} (F_{\text{vis}}(r) + F_{\text{acc}}(r) \right. \\ &\quad \left. + k_s F_P(r)) + T_{\text{neb}}^4}{\sigma_{\text{SB}}} \right)^{1/4} , \end{aligned} \quad (13)$$

where

$$\begin{aligned} F_{\text{vis}}(r) &= \frac{3}{8\pi} \frac{\Lambda(r)}{l} \dot{M} \Omega_K(r)^2 \\ F_{\text{acc}}(r) &= \frac{X_d \chi G M_p \dot{M}}{4\pi r_c^2 r} e^{-(r/r_c)^2} \\ F_P(r) &= L_P \frac{\sin(\zeta(r)r + \eta(r))}{8\pi(r^2 + z_s^2)} \end{aligned} \quad (14)$$

are the energy fluxes from viscous heating, accretion onto the disk, and the planetary illumination, and  $T_{\text{neb}}$  denotes the background temperature of the circumstellar nebula (100 K in our simulations). The geometry of the flaring disk is expressed by the angles

$$\begin{aligned} \zeta(r) &= \arctan\left(\frac{4}{3\pi} \frac{R_p}{\sqrt{r^2 + z_s^2}}\right) \\ \eta(r) &= \arctan\left(\frac{dz_s}{dr}\right) - \arctan\left(\frac{z_s}{r}\right) . \end{aligned} \quad (15)$$

Taking into account the radiative transfer within the optically thick disk with Planck opacity  $\kappa_P$ , the midplane temperature can be estimated as ([Makalkin & Dorofeeva 2014](#))

$$\begin{aligned} T_m(r)^5 - T_s(r)^4 T_m(r) &= \frac{12\mu\chi\kappa_P}{2^9\pi^2\sigma_{\text{SB}}R_g\gamma} \times \frac{\dot{M}^2}{\alpha} \Omega_K(r)^3 \\ &\quad \times \left(\frac{\Lambda(r)}{l}\right)^2 q_s(r)^2 , \end{aligned} \quad (16)$$

where  $\sigma_{\text{SB}}$  is the Stefan-Boltzmann constant,  $R_{\text{Gas}}$  the ideal gas constant,  $\gamma = 1.45$  the adiabatic exponent (or ratio of the heat capacities), and

$$q_s(r) = 1 - \frac{4}{3\kappa_P \Sigma_g(r)}$$

is the vertical mass coordinate at  $z_s$ .

## 2.2. Planet Evolution Tracks

We use a pre-computed grid of planet formation models by [Mordasini \(2013\)](#) to feed our planet disk model with the fundamental planetary properties such as the planet's evolving radius ( $R_p$ ), its mass, mass accretion rate ( $\dot{M}_p$ ), and luminosity ( $L_p$ ). Figure 1 shows the evolution of these quantities with black solid lines indicating an accreting gas giant that ends up with one Jupiter mass or about 318 Earth masses ( $M_{\oplus}$ ). In total, we have seven models at our disposal, where the planets have final masses of 1, 2, 3, 5, 7, 10, and 12  $M_{\text{Jup}}$ . These tracks are sensitive to the planet's core mass, which we assume to be 33  $M_{\oplus}$  for all planets. Jupiter's core mass is actually much lower, probably around 10  $M_{\oplus}$  ([Guillot et al. 1997](#)). Lower final core masses in these models translate into lower planetary luminosities at any given accretion rate. In other words, our results for the H<sub>2</sub>O ice lines around the Jupiter-mass test planet are actually upper,

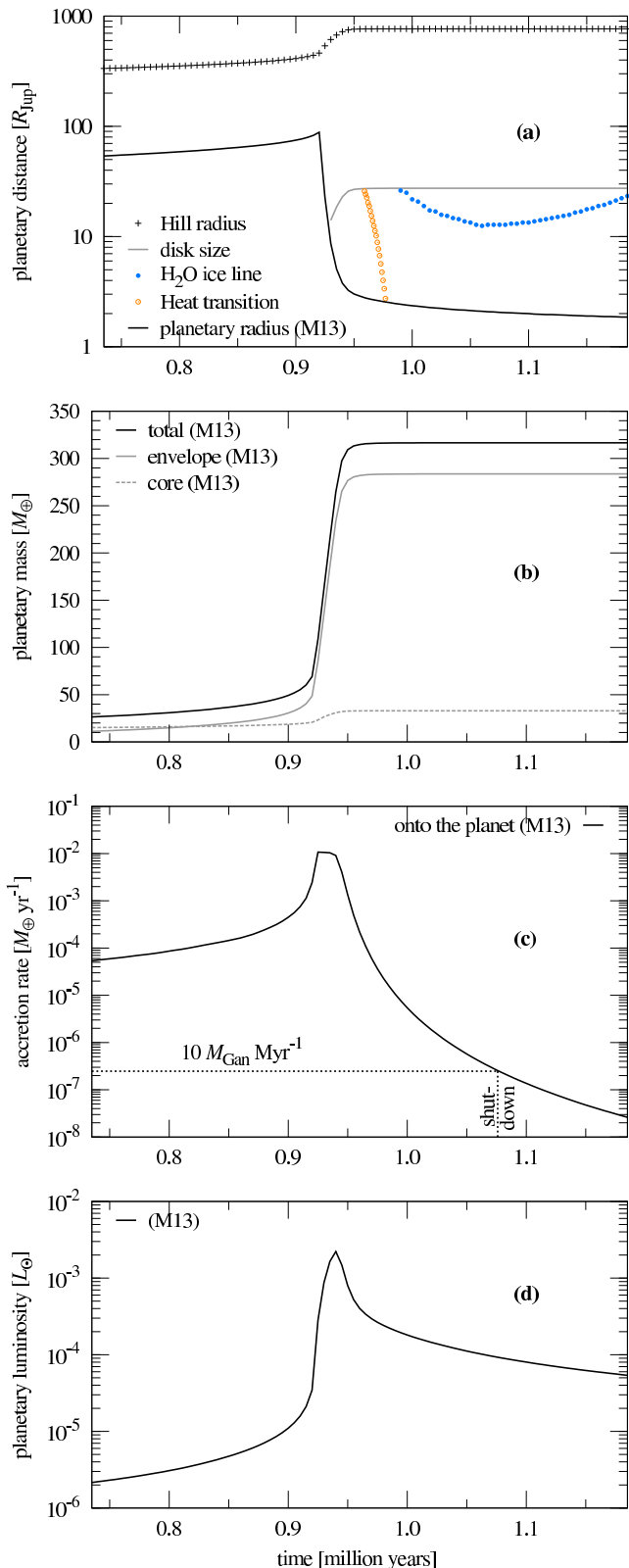


**Figure 1.** Evolution of a Jupiter-like model planet and its circumplanetary disk. Values taken from [Mordasini \(2013\)](#) are labeled “M13”. (A) Circumplanetary disk properties. (B) Growth of the solid core, gaseous envelope, and total mass. (C) Total mass accretion rate. The dashed horizontal line indicates our fiducial shutdown rate for moon formation of  $10 M_{\text{Gan}} \text{ Myr}^{-1}$ . The dashed vertical line marks the corresponding shutdown for moon formation at about  $1.08 \times 10^6 \text{ yr}$ . (D) Planetary luminosity evolution.

or outer limits, and a more realistic evaluation of the conditions around Jupiter would shift the ice lines closer to the planet. Over the whole range of available planet tracks with core masses between  $22$  and  $130 M_{\oplus}$ , we note that the planetary luminosities at shutdown are  $10^{-4.11}$  and  $10^{-3.82}$  solar luminosities, respectively. As the distance of the  $\text{H}_2\text{O}$  ice line in a radiation-dominated disk scales with  $L_p^{1/2}$ , different planetary core masses would thus affect our results by less than ten percent.

The pre-computed planetary models cover the first few  $10^6 \text{ yr}$  after the onset of accretion onto the planet. We interpolate all quantities on a discrete time line with a step size of  $5,000 \text{ yr}$ . At any given time, we feed Equations (14) with the planetary model and solve the coupled Equations (1)-(10) in an iterative framework. With  $T_s$  provided by Equation (13), we finally solve the 5th order polynomial in Equation (16) numerically.

Once the planetary evolution models indicate that the planet’s mass accretion has dropped below a critical shutdown accretion rate ( $\dot{M}_{\text{shut}}$ ), we assume that the formation of satellites has effectively stopped. As an example, no Ganymede-sized moon can form once  $\dot{M}_{\text{shut}} < M_{\text{Gan}}/(10^6 \text{ yr})$  ( $M_{\text{Gan}}$  being the mass of Ganymede) and if the disk’s remaining life time is  $< 10^6 \text{ yr}$  (see Figure 1, panel C).

In any single simulation run,  $\kappa_P$  is assumed to be constant throughout the disk, and simulations of the planetary  $\text{H}_2\text{O}$  ice lines are terminated once the planet accretes less than a given  $\dot{M}_{\text{shut}}$ . To obtain a realistic picture of a broad range of hypothetical exoplanetary disk properties, we ran a suite of randomized simulations, where  $\kappa_P$  and  $\dot{M}_{\text{shut}}$  were drawn from a lognormal probability density distribution. For  $\log_{10}(\kappa_P/[\text{m}^2 \text{ kg}^{-1}])$  we assumed a mean value of  $-2$  and a standard variation of  $1$ , and concerning the shutdown accretion rate we assumed a mean value of  $1$  for  $\log_{10}(\dot{M}_{\text{shut}}/[M_{\text{Gan}} \text{ Myr}^{-1}])$  and a standard variation of  $1$ .

To get a handle on the plausible surface absorptivities of various disk, we tested different values of  $k_s$  between  $0.1$  and  $0.5$ . For each of the seven test planets, we performed 120 randomized simulations of the disk evolution and then calculated the arithmetic mean distance of the final water ice line. The resulting distributions are skewed and non-Gaussian. Hence, we compute both the downside and the upside semi standard deviation (corresponding to  $\sigma/2$ ), that is, the distance ranges that comprise  $+68.3\%/2 = +34.15\%$  and  $-34.15\%$  of the simulations around the mean. We also calculate the  $2\sigma$  semi-deviation, corresponding to  $+95.5\%/2 = +47.75\%$  and  $-47.75\%$  around the mean. Downside and upside semi deviations combined deliver an impression of the asymmetric deviations from the mean, and their sum equals that of the Gaussian standard deviations.

The total, instantaneous mass of solids in the disk at the time of moon formation shutdown is given as

$$M_s = 2\pi X \left( \int_{r_{\text{in}}}^{r_{\text{ice}}} dr r \Sigma_g(r) + 3 \int_{r_{\text{ice}}}^{r_{\text{cf}}} dr r \Sigma_g(r) \right), \quad (17)$$

where  $r_{\text{in}}$  is the inner truncation radius of the disk (assumed at Jupiter’s corotation radius of  $2.25 R_{\text{Jup}}$ , [Camup & Ward 2002](#)),  $r_{\text{ice}}$  is the distance of the  $\text{H}_2\text{O}$  ice line, and  $r_{\text{cf}}$  is the outer, centrifugal radius of the disk ([Machida](#)

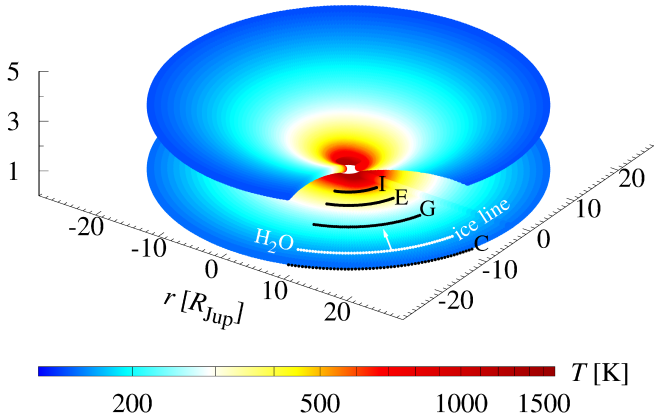


**Figure 2.** Disk temperatures around a forming Jupiter-like planet  $10^6$  yr after the onset of accretion. The two disk levels represent the midplane and the photosphere (at a high  $z_s$  above the midplane). At a given radial distance ( $r$ ) to the planet, measured in Jupiter radii, the midplane is usually warmer than the surface (see color bar). The orbits of Io, Europa, Ganymede, and Callisto (labelled I, E, G, and C, respectively) and the location of the instantaneous  $\text{H}_2\text{O}$  ice line at  $\approx 22.5 R_{\text{Jup}}$  are indicated in the disk midplane. The arrow attached to the ice line indicates that it is still moving inward before it reaches its final location at roughly the orbit of Ganymede. This simulation assumes fiducial disk values ( $k_s = 0.2$ ,  $\kappa_P = 10^{-2} \text{ m}^2 \text{ kg}^{-1}$ ), some  $10^5$  yr before the shutdown of moon formation.

et al. 2008). Depending on the density of the disk gas and the size of the solid grains, the water sublimation temperature can vary by several degrees Kelvin (Lewis 1972; Lecar et al. 2006), but we adopt 170 K as our fiducial value (Hasegawa & Pudritz 2013).

We simulate the evolution of the  $\text{H}_2\text{O}$  ice lines in the disks around young super-Jovian planets at 5.2 astronomical units (AU, the distance between the Sun and the Earth) from a Sun-like star, facilitating comparison of our results to the Jovian moon system. These planets belong to the observed population of super-Jovian planets at  $\approx 1$  AU around Sun-like stars (Hasegawa & Pudritz 2011, 2012; Howard 2013), and it has been shown that their satellite systems may remain intact during planet migration (Namouni 2010).

### 3. RESULTS AND PREDICTIONS

Figure 1(A) shows, on the largest radial scales, the Hill radius of the accreting giant planet. The planetary radius is well within the Hill sphere, but it is quite extensive for 0.9 Myr, so much so that the disk has not yet appeared by that time. The circumplanetary accretion disk only appears after 0.9 Myr of evolution of the system. Within the disk, we follow the time evolution of two features – the heat transition and the  $\text{H}_2\text{O}$  ice line. The appearance of a heat transition (orange open circles), which is the transition from the viscous to the irradiation heating regime in the disk, at the outer disk edge (see Hasegawa & Pudritz 2011), about  $0.95 \times 10^6$  yr after the onset of accretion. It moves rapidly inwards and within  $\approx 2 \times 10^4$  yr it reaches the inner disk edge, which sits roughly at the radius of the planet (solid line). At the same time ( $\approx 0.99 \times 10^6$  yr after the onset of accretion), the  $\text{H}_2\text{O}$  ice line (blue dots) appears at the outer disk radius and then moves slowly inward as the planet cools. The ice line reverses its direction of movement at  $\approx 1.1 \times 10^6$  yr due to the decreasing gas surface densities, while the opacities are assumed to be constant

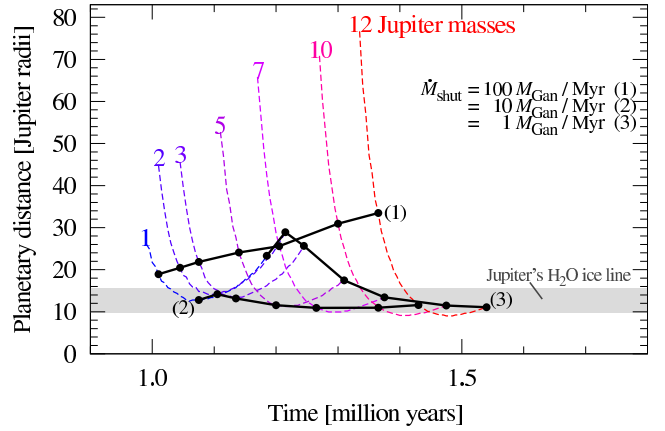


**Figure 3.** Evolution of the  $\text{H}_2\text{O}$  ice lines in the disks around super-Jovian gas planets. Black solid lines, labeled (1) - (3), indicate the locations of the  $\text{H}_2\text{O}$  ice lines assuming different mass accretion rates for the shutdown of moon formation ( $M_{\text{shut}} \in \{100, 10, 1\} \times M_{\text{Gan}}/10^6 \text{ yr}$ ). The shaded area embraces the orbits of Europa and Ganymede around Jupiter, where Jupiter's  $\text{H}_2\text{O}$  ice line must have been at the time when the Galilean satellites completed formation. The most plausible shutdown rate for the Jovian system (black line with label 2) predicts ice lines between roughly 10 and  $15 R_{\text{Jup}}$  over the whole range of super-Jovian planetary masses. Simulations assume  $k_s = 0.2$  and  $\kappa_P = 10^{-2} \text{ m}^2 \text{ kg}^{-2}$ .

throughout the disk, see Equation (13). Panel (B) displays the mass accretion of the planetary core and atmosphere. Note that the rapid accumulation of the envelope and the total mass at around  $0.93 \times 10^6$  yr corresponds to the runaway accretion phase. Panel (C) presents the total mass accretion rate onto the planet (black solid line). The dashed horizontal line shows an example for  $M_{\text{shut}}$  (here  $10 M_{\text{Gan}} \text{ Myr}^{-1}$ ), which corresponds to a time 1.08 Myr after the onset of accretion in that particular model. Note that shutdown accretion rates within one order of magnitude around this fiducial value occur 0.1 - 0.3 Myr after the runaway accretion phase, that is, after the planet has opened up a gap in the circumstellar disk. In panel (D), the planetary luminosity peaks during the runaway accretion phase and then dies off as the planet opens up a gap in the circumstellar disk, which starves the circumplanetary disk.

Figure 2 shows a snapshot of the temperature structure of the disk surface and midplane around a Jupiter-mass planet,  $10^6$  yr after the onset of mass accretion. The location of the instantaneous water ice line is indicated with a white dotted line, and the current positions of the Galilean satellites are shown with black dotted lines. Over the next hundred thousand years, the heating rates drop and the ice line moves inward to Ganymede's present orbit as the planet's accretion rate decreases due to its opening of a gap in the circumstellar disk. We argue that the growing Ganymede moved with the ice line trap and was parked in its present orbit when the circumjovian disk dissipated. Due to the rapid decrease of mass accretion onto the planet after gap opening (up to about an order of magnitude per  $10^4$  yr), this process can be reasonably approximated as an instant shutdown on the time scales of planet formation (several  $10^6$  yr), although it is truly a gradual process.

Figure 3 shows the radial positions of the ice lines around super-Jovian planets as a function of time and for a given disk surface absorptivity ( $k_s$ ) and disk Planck opacity ( $\kappa_P$ ). More massive planets have larger disks

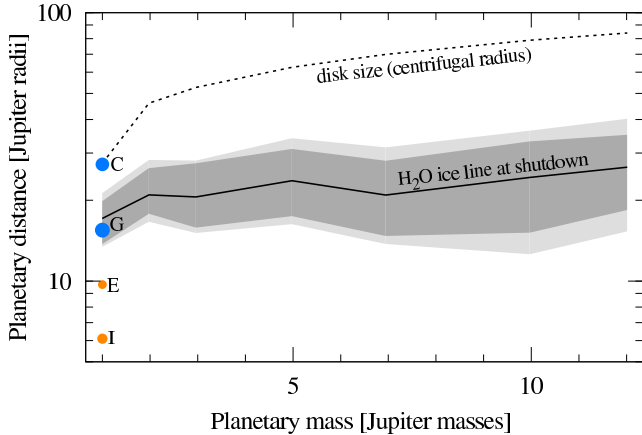


**Figure 4.** Distance of the H<sub>2</sub>O ice lines at the shutdown of moon formation around super-Jovian planets. The solid line indicates the mean, while shaded areas denote the statistical scatter (dark gray 1  $\sigma$ , light gray 2  $\sigma$ ) in our simulations, based on the posterior distribution of the disk Planck mean opacity ( $\kappa_P$ ) and the shutdown accretion rate for moon formation ( $\dot{M}_{\text{shut}}$ ). The dashed line represents the size of the optically thick part of the circumplanetary disk, or its centrifugal radius. All planets are assumed to orbit a Sun-like star at a distance of 5.2 AU and  $k_s$  is set to 0.2. Labeled circles at 1  $M_{\text{Jup}}$  denote the orbits of the Galilean satellite Io, Europa, Ganymede, and Callisto. Orange indicates rocky composition, blue represents H<sub>2</sub>O-rich composition. Circle sizes scale with moon radii. Note that Ganymede sits almost exactly on the circum-Jovian ice line.

and are also hotter at a given time after the onset of accretion, which explains the larger distance and later occurrence of water ice around the more massive giants. Solid black lines connect epochs of equal accretion rates (1, 10, and 100  $M_{\text{Gan}}$  per  $10^6$  yr). Along any given ice line track, higher accretion rates correspond to earlier phases. The H<sub>2</sub>O ice line around the 1 Jupiter mass model occurs after  $\approx 0.99 \times 10^6$  yr at the outer edge of the disk, passes through the current orbit of Ganymede, and then begins to move outwards around  $\approx 1.1 \times 10^6$  yr due to the decreasing gas surface densities (note, the opacities are assumed constant). In this graph,  $\dot{M}_{\text{shut}} \approx 10 M_{\text{Gan}} / (10^6 \text{ yr})$  can well explain the mentioned properties in the Galilean system.

In Figure 4, we present the locations of the ice lines in a more global picture, obtained by performing 120 randomized disk simulations for each planet, where  $\dot{M}_{\text{shut}}$  and  $\kappa_P$  were drawn from a lognormal probability distribution. We also simulated several plausible surface absorptivities of the disk (D’Alessio et al. 2001; Makalkin & Dorofeeva 2014) ( $0.1 \leq k_s \leq 0.5$ ), which resulted in ice line locations similar to those shown in Figure 4, where  $k_s = 0.2$ . The mean orbital radius of the ice line at the time of shutdown around the 1  $M_{\text{Jup}}$  planet is almost precisely at Ganymede’s orbit around Jupiter, which we claim is no mere coincidence. Most importantly, despite a variation of  $\dot{M}_{\text{shut}}$  by two orders of magnitude and considering more than one order of magnitude in planetary masses, the final distances of the H<sub>2</sub>O ice lines only vary between about 15 and 30  $R_{\text{Jup}}$ . Hence, regardless of the actual value of  $\dot{M}_{\text{shut}}$ , the transition from rocky to icy moons around giant planets at several AU from Sun-like stars should occur at planetary distances similar to the one observed in the Galilean system. We ascribe this result to the fact that the planetary luminosity is the dominant heat source at the time of moon formation shutdown.

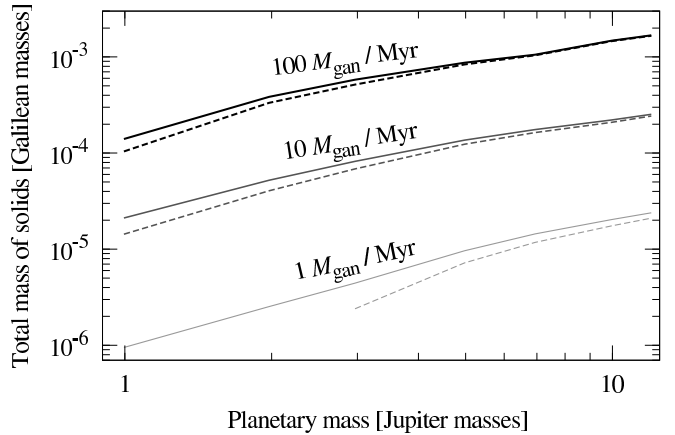


**Figure 5.** Instantaneous mass of solids in the disks around super-Jovian planets at moon formation shutdown. Solid and dashed lines refer to disk absorptivities of  $k_s = 0.2$  and 0.4, respectively. The ordinate scales in units of the total mass contained in the Galilean moons ( $\approx 2.65 M_{\text{Gan}}$ ). For any given shutdown rate, we find a linear increase in the mass of solids at the time of moon formation shutdown as a function of planetary mass, in agreement with previous simulations for the solar system giants (Canup & Ward 2006; Sasaki et al. 2010). Super-Jovian planets of 10  $M_{\text{Jup}}$  should thus have moon systems with total masses of  $\approx 10^{-3} \times M_{\text{Jup}}$ , or 3 times the mass of Mars.

Planetary luminosity, in turn, is determined by accretion (and gravitational shrinking), hence a given  $\dot{M}_{\text{shut}}$  translates into similar luminosities and similar ice line radii for all super-Jovian planets. Planets above 1  $M_{\text{Jup}}$  have substantially larger parts of their disks beyond their water ice lines (note the logarithmic scale in Figure 4) and thus have much more material available for the formation of giant, water-rich analogs of Ganymede and Callisto.

Figure 5 shows the total mass of solids at the time of moon formation shutdown around super-Jovian planets. Intriguingly, for any given shutdown accretion rate the total mass of solids scales proportionally to the planetary mass. This result is not trivial, as the mass of solids depends on the location of the H<sub>2</sub>O ice line at shutdown. Assuming that  $\dot{M}_{\text{shut}}$  is similar among all super-Jovian planets, we confirm that the  $M_{\text{T}} \propto 10^{-4} M_{\text{p}}$  scaling law observed in the solar system also applies for extrasolar super-Jupiters (Canup & Ward 2006; Sasaki et al. 2010).

In addition to the evolution of the H<sub>2</sub>O ice lines, we also tracked the movements of the heat transitions, a specific location within the disk, where the heating from planetary irradiation is superseded by viscous heating. Heat transitions cross the disk within only about  $10^4$  yr (see Figure 1, panel A), several  $10^5$  yr before the shutdown of moon formation, and thereby cannot possibly act as moon traps. Their rapid movement is owed to the abrupt starving of the planetary disk due to the gap opening of the circumstellar disk, whereas the much slower photoevaporation of the latter yields a much slower motion of the circumstellar heat trap. The ineffectiveness of heat traps for satellites reflects a key distinction between the processes of moon formation and terrestrial planet formation.

#### 4. DISCUSSION

A key distinction between our own work and previous models is in the question of the role of type I migration. Other models assume that type I migration of the forming moons leads to a continuous rapid loss

of proto-satellites into the planet (Canup & Ward 2002; Sasaki et al. 2010) and that the Galilean moons around Jupiter must have built in the late, low-density accretion disk, where type I migration was negligible (Alibert et al. 2005). The latter authors considered Jupiter’s accretion disk as a closed system after the circumstellar accretion disk had been photo-evaporated.

There are two difficulties with such a picture. First, type I migration can be drastically slowed down as growing giant moons get trapped by the ice lines. Thus it is not obvious that a conveyor belt of moons into their host planets is ever established. Second, our Figure 5 also contradicts this scenario, because the instantaneous mass of solids in the disk during the end stages of moon formation (or planetary accretion) is not sufficient to form the last generation of moons. In other words, whenever the instantaneous mass of solids contained in the circum-Jovian disk was similar to the total mass of the Galilean moons, the correspondingly high accretion rates caused the H<sub>2</sub>O ice line to be far beyond the orbits of Europa and Ganymede.

We infer, therefore, that the final moon population around Jupiter and other Jovian or super-Jovian exoplanets must, at least to a large extent, have built during the ongoing, final accretion process of the planet, when it was still fed from the circumstellar disk. In order to counteract the inwards flow due to type I migration, we suggest a new picture in which the circumplanetary H<sub>2</sub>O ice line has acted as a migration trap. This important hypothesis needs to be tested in future studies.

We can extend our argument to address the origin of the entire Jovian moon system. In our picture, Io should have formed dry. It did not form wet and then lose its water through tidal heating. Ganymede may have formed at the water ice line in the circumjovian disk, where it has forced Io and Europa in the 1:2:4 orbital mean motion resonance (Laplace et al. 1829). From a formation point of view, we suggest that Io and Europa be regarded as moon analogs of the terrestrial planets, whereas Ganymede and Callisto resemble the rapidly growing precursors of giant planets.

Finally, we must address a technical issue, namely, our choice of the  $\alpha$  parameter ( $10^{-3}$ ). While this is consistent with many previous studies, how would a variation of  $\alpha$  change our results? Magnetorotational instabilities might be restricted to the upper layers of circumplanetary accretion disks, where they become sufficiently ionized (mostly by cosmic high-energy radiation and stellar X-rays). Magnetic turbulence and viscous heating in the disk midplane might thus be substantially lower than in our model (Fujii et al. 2014). On the other hand, Gressel et al. (2013) modeled the magnetic stresses in circumplanetary disks with a 3D magnetohydrodynamic model and inferred  $\alpha$  values of 0.01 and larger, which would strongly enhance viscous heating. Obviously, sophisticated numerical simulations of giant planet accretion do not yet consistently describe the magnetic properties of the disks and the associated  $\alpha$  values. Given that circumstellar disks are almost certainly magnetized, circumplanetary disks can be expected to have inherited magnetic fields from this source. This makes it likely that magnetized disk winds can be driven off the circumplanetary disks (Fendt 2003; Pudritz et al. 2007) which can carry significant amounts of angular momentum. Even

in the limit of very low ionization, Bai & Stone (2013) demonstrated that magnetized disk winds will transport disk angular momentum at the rates needed to allow accretion onto the central object. However, independent of these uncertainties, the final positions of the H<sub>2</sub>O ice line produced in our simulations turn out to depend mostly on planetary illumination, because viscous heating becomes negligible almost immediately following gap opening. Hence, even substantial variations of  $\alpha$  by a factor of ten would hardly change our results for the ice line locations at moon formation shutdown since these must develop in radiatively dominated disk structure (but it would alter them substantially in the viscous-dominated regime before and during runaway accretion).

## 5. CONCLUSIONS

We have demonstrated that ice lines imprint important structural features on the system of icy moons around massive planets. Given that the data shows a strong concentration of super-Jovian planets at  $\approx 1$  AU, we focused our analysis on the formation of massive moons in this planetary population at these characteristic orbital radii.

Our model confirms the mass scaling law for these most massive planets which suggests that satellite systems with total masses several times the mass of Mars await discovery. Their most massive members will be rich in water and possibly parked in orbits at their host planet’s H<sub>2</sub>O ice lines at the time of moon formation shutdown, that is, between 15 and 30 Jupiter radii from the planet. A Mars-mass moon composed of 50 % of water would have a radius of  $\approx 0.7$  Earth radii (Fortney et al. 2007). Although we considered giant planet accretion beyond 1 AU, super-Jovian planets are most abundant around 1 AU (Howard 2013) and their moon systems have been shown to remain intact during planet migration (Namouni 2010). Giant water-rich moons might therefore form an abundant population of extrasolar habitable worlds (Williams et al. 1997; Heller et al. 2014) and their sizes could make them detectable around photometrically quiet dwarf stars with the transit method (Kipping et al. 2012; Heller 2014). In a few cases, the transits of such giant moons in front of hot, young giant planets might be detectable with the European Extremely Large Telescope, with potential for follow-up observations of the planetary Rossiter-McLaughlin effect (Heller & Albrecht 2014).

More detailed predictions can be obtained by including the migration process of the accreting planet, which we will present in an upcoming paper. Ultimately, we expect that there will be a competition between the formation of water-rich, initially icy moons beyond the circumplanetary H<sub>2</sub>O ice line and the gradual heating of the disk (and loss of ices) during the planetary migration towards the star. Such simulations have the potential to generate a moon population synthesis with predictions for the abundance and detectability of large, water-rich moons around super-Jovian planets.

We thank C. Mordasini for sharing with us his planet evolution tracks, G. D’Angelo for discussions related to disk ionization, and A. Makalkin for advice on the disk properties. René Heller is supported by the Origins Insti-

tute at McMaster University and by the Canadian Astrobiology Program, a Collaborative Research and Training Experience Program funded by the Natural Sciences and Engineering Research Council of Canada (NSERC). REP is supported by a Discovery grant from NSERC.

## REFERENCES

- Alibert, Y., Mousis, O., & Benz, W. 2005, *A&A*, 439, 1205  
 Bai, X.-N., & Stone, J. M. 2013, *ApJ*, 769, 76  
 Barclay, T., Rowe, J. F., Lissauer, J. J., et al. 2013, *Nature*, 494, 452  
 Canup, R. M., & Ward, W. R. 2002, *AJ*, 124, 3404  
 —. 2006, *Nature*, 441, 834  
 Crida, A., & Charnoz, S. 2012, *Science*, 338, 1196  
 D’Alessio, P., Calvet, N., & Hartmann, L. 2001, *ApJ*, 553, 321  
 Fendt, C. 2003, *A&A*, 411, 623  
 Fortney, J. J., Marley, M. S., & Barnes, J. W. 2007, *ApJ*, 659, 1661  
 Fujii, Y. I., Okuzumi, S., Tanigawa, T., & Inutsuka, S.-i. 2014, *ApJ*, 785, 101  
 Gressel, O., Nelson, R. P., Turner, N. J., & Ziegler, U. 2013, *ApJ*, 779, 59  
 Guillot, T., Gautier, D., & Hubbard, W. B. 1997, *Icarus*, 130, 534  
 Hasegawa, Y., & Pudritz, R. E. 2011, *MNRAS*, 417, 1236  
 —. 2012, *ApJ*, 760, 117  
 —. 2013, *ApJ*, 778, 78  
 Hayashi, C. 1981, *Progress of Theoretical Physics Supplement*, 70, 35  
 Heller, R. 2014, *ApJ*, 787, 14  
 Heller, R., & Albrecht, S. 2014, *ArXiv e-prints*  
 Heller, R., Williams, D., Kipping, D., et al. 2014, *Astrobiology*, 14, 798  
 Howard, A. W. 2013, *Science*, 340, 572  
 Keith, S. L., & Wardle, M. 2014, *MNRAS*, 440, 89  
 Kipping, D. M., Bakos, G. Á., Buchhave, L., Nesvorný, D., & Schmitt, A. 2012, *ApJ*, 750, 115  
 Kretke, K. A., & Lin, D. N. C. 2007, *ApJ*, 664, L55  
 Laplace, P. S., Bowditch, N., & Bowditch, N. I. 1829, *Mécanique céleste*  
 Lecar, M., Podolak, M., Sasselov, D., & Chiang, E. 2006, *ApJ*, 640, 1115  
 Lewis, J. S. 1972, *Icarus*, 16, 241  
 Lissauer, J. J., Hubickyj, O., D’Angelo, G., & Bodenheimer, P. 2009, *Icarus*, 199, 338  
 Machida, M. N., Kokubo, E., Inutsuka, S.-i., & Matsumoto, T. 2008, *ApJ*, 685, 1220  
 Makalkin, A. B., & Dorofeeva, V. A. 1995, *Solar System Research*, 29, 85  
 —. 2014, *Solar System Research*, 48, 62  
 Mordasini, C. 2013, *A&A*, 558, A113  
 Mosqueira, I., & Estrada, P. R. 2003, *Icarus*, 163, 198  
 Mousis, O., & Gautier, D. 2004, *Planet. Space Sci.*, 52, 361  
 Namouni, F. 2010, *ApJ*, 719, L145  
 Ogihara, M., & Ida, S. 2012, *ApJ*, 753, 60  
 Pollack, J. B., & Reynolds, R. T. 1974, *Icarus*, 21, 248  
 Pudritz, R. E., Ouyed, R., Fendt, C., & Brandenburg, A. 2007, *Protostars and Planets V*, 277  
 Sasaki, T., Stewart, G. R., & Ida, S. 2010, *ApJ*, 714, 1052  
 Showman, A. P., & Malhotra, R. 1999, *Science*, 286, 77  
 Williams, D. M., Kasting, J. F., & Wade, R. A. 1997, *Nature*, 385, 234